JOURNAL OF MODERN OPTICS, 2016
VOL. 63, NO. 15, 1429–1437
http://dx.doi.org/10.1080/09500340.2016.1151565

Taylor & Francis
Taylor & Francis Group

The tight focusing properties of Laguerre–Gaussian-correlated Schell-model beams

Hua-Feng Xu[a,b], Zhou Zhang[a], Jun Qu[c] and Wei Huang[a,b]

[a]Laboratory of Atmospheric Physico-Chemistry, Anhui Institute of Optics & Fine Mechanics, Chinese Academy of Sciences, Hefei, China; [b]University of Science and Technology of China, Hefei, China; [c]Department of Physics, Anhui Normal University, Wuhu, China

ABSTRACT

Based on the Richards–Wolf vectorial diffraction theory, the tight focusing properties, including the intensity distribution, the degree of polarization and the degree of coherence, of the Laguerre–Gaussian-correlated Schell-model (LGSM) beams through a high-numerical-aperture (NA) focusing system are investigated in detail. It is found that the LGSM beam exhibits some extraordinary focusing properties, which is quite different from that of the GSM beam, and the tight focusing properties are closely related to the initial spatial coherence δ_g and the mode order n. The LGSM beam can form an elliptical focal spot, a circular focal spot or a doughnut-shaped dark hollow beam at the focal plane by choosing a suitable value of the initial spatial coherence δ_g, and the central dark size of the dark hollow beam increases with the increase of the mode order n. In addition, the influences of the initial spatial coherence δ_g and the mode order n on the degree of polarization and the degree of coherence are also analysed in detail, respectively. Our results may find applications in optical trapping.

ARTICLE HISTORY
Received 16 November 2015
Accepted 1 February 2016

KEYWORDS
Partially coherent beams; focusing properties; polarization; coherence

1. Introduction

Over the past decades, partially coherent beams with conventional correlation functions (i.e. Gaussian-correlated Schell-model functions) have drawn considerable attention due to their wide applications in free-space optical communications, optical trapping, remote sensing and optical imaging and so on [1–7]. It is well known that the partially coherent beams have advantage over the fully coherent beams for overcoming or reducing the turbulence-induced degradation [2–4]. Since the sufficient condition for devising a genuine correlation function of scalar and electromagnetic partially coherent source was established by Gori and collaborators [8,9], the study on the partially coherent beams with nonconventional correlation functions has become a hot topic. In recent years, a variety of partially coherent beams with special correlation functions have been introduced and studied both theoretically and experimentally, such as nonuniformly correlated beams [10–14], multi-Gaussian-correlated Schell-model beams [15–19], Laguerre–Gaussian-correlated Schell-model (LGSM) beams of circular or elliptical symmetry [20–25], Bessel–Gaussian-correlated Schell-model beams [20,26], cosine-Gaussian-correlated Schell-model beams of circular or rectangular symmetry [26–33], Hermite–Gaussian-correlated Schell-model beams [34], special correlated partially coherent vector beams [35], sinc Schell-model beams [36,37], etc. The experimental generation of such random beams can be realized using the nematic spatial light modulator [13,22–24,26,29,34,35]. In addition, propagation properties of those beams in turbulent atmosphere were explored, and it was found that those partially coherent beams with special correlation functions exhibit some extraordinary characteristics on propagation, such as far-field flat-topped or ring-shaped beam profile formation [15,16,20,27], self-focusing or self-splitting effect [10,14,28,31,34], lateral shift of the intensity maximum [10,11,14], and controllable optical cage formation near the focal plane [22]. Furthermore, it has been revealed that, compared with the GSM beams, the partially coherent beams with special correlation functions have the potential ability to further improving the performance of laser beams' propagation [18,21,33], which will be useful for free-space optical communications.

On the other hand, the study on the tight focusing properties of various beams through an aplanatic high-numerical-aperture (NA) focusing system is always a subject

CONTACT Jun Qu qujun70@mail.ahnu.edu.cn; Wei Huang huangwei6@ustc.edu.cn

© 2016 Informa UK Limited, trading as Taylor & Francis Group

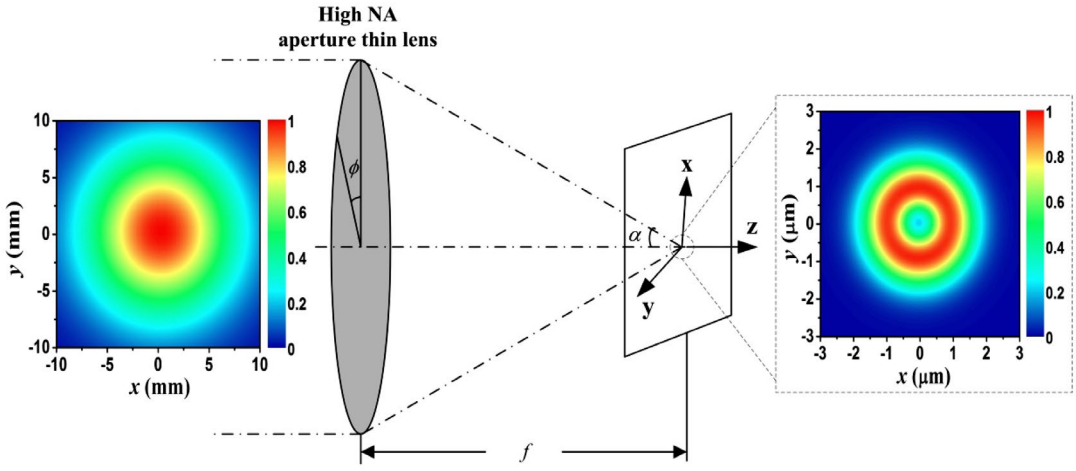

Figure 1. Scheme of the tight focusing system. Left and right plots are the intensity distribution of the LGSM beam at the input and focal planes, respectively. (The colour version of this figure is included in the online version of the journal.)

of great interest due to its practical applications in optical trapping, laser maching, and high-resolution imaging. Up to now, the tight focusing properties of various beams, such as cylindrical vector beams, vortex beams, partially coherent beams with conventional correlation functions, have been widely studied [6,38–47]. However, to the best of our knowledge, the tight focusing properties of the partially coherent beams with nonconventional correlation functions through a high-NA focusing system have not been reported. The main purpose of this paper is to study the tight focusing properties, including the intensity distribution, the degree of polarization, and the degree of coherence, of a linearly polarized LGSM beam through an aplanatic high-NA focusing system. The influence of the initial spatial coherence δ_g and the mode order n on the tight focusing properties is discussed in detail. Some interesting and useful results are found.

2. Theory

In the rectangular coordinate system, the cross-spectral density (CSD) of the LGSM beam at the source plane ($z = 0$) can be expressed as [20,22,25]:

$$W^{(0)}(\mathbf{r}_1,\mathbf{r}_2) = \exp\left[-\frac{\mathbf{r}_1^2+\mathbf{r}_2^2}{4\sigma_0^2} - \frac{(\mathbf{r}_2-\mathbf{r}_1)^2}{2\delta_g^2}\right] L_n^0\left[\frac{(\mathbf{r}_2-\mathbf{r}_1)^2}{2\delta_g^2}\right] \tag{1}$$

where $\mathbf{r}_1 \equiv (x_1, y_1)$ and $\mathbf{r}_2 \equiv (x_2, y_2)$ are two arbitrary transverse position vectors in the source plane, σ_0 is the beam width and δ_g denotes the spatial coherence length. $L_n^0(\cdot)$ represents the Laguerre polynomial of mode order n and 0. For simplicity, the angular frequency dependence of all the quantities of interest is omitted. The source degree of coherence of the LGSM beam at the plane of $z = 0$ can be described as [20,22,25]

$$\mu^{(0)}(\mathbf{r}_1,\mathbf{r}_2) = \frac{W^{(0)}(\mathbf{r}_1,\mathbf{r}_2)}{\sqrt{W^{(0)}(\mathbf{r}_1,\mathbf{r}_1)W^{(0)}(\mathbf{r}_2,\mathbf{r}_2)}} = \exp\left[-\frac{(\mathbf{r}_1-\mathbf{r}_2)^2}{2\delta_g^2}\right] L_n^0\left[\frac{(\mathbf{r}_1-\mathbf{r}_2)^2}{2\delta_g^2}\right] \tag{2}$$

It is clear from Equation (2) that the source degree of coherence of the LGSM beam is modulated by the Laguerre function, and presents a non-Gaussian distribution for $n \neq 0$. While for $n = 0$, it reduces to that of the conventional GSM source.

By use of the following relation between the rectangular coordinates and the cylindrical coordinates,

$$\begin{aligned} x_1 &= r_1\cos\varphi_1, y_1 = r_1\sin\varphi_1, \\ x_2 &= r_2\cos\varphi_2, y_2 = r_2\sin\varphi_2, \end{aligned} \tag{3}$$

then, the CSD function of the LGSM beam in the source plane can be expressed in the following form

$$W(r_1,\varphi_1,r_2,\varphi_2) = \exp\left[-\frac{r_1^2+r_2^2}{4\sigma_0^2} - \frac{r_1^2+r_2^2-2r_2r_1\cos(\varphi_1-\varphi_2)}{2\delta_g^2}\right] \times L_n^0\left[\frac{r_1^2+r_2^2-2r_2r_1\cos(\varphi_1-\varphi_2)}{2\delta_g^2}\right] \tag{4}$$

Now, we consider a linearly polarized LGSM beam focused by a high-NA thin lens in free space, as shown in (Figure 1). As an interesting example, a LGSM beam with quasi-Gaussian intensity profile in front of the lens focusing into a circular dark hollow beam at the focal plane is also shown in (Figure 1).

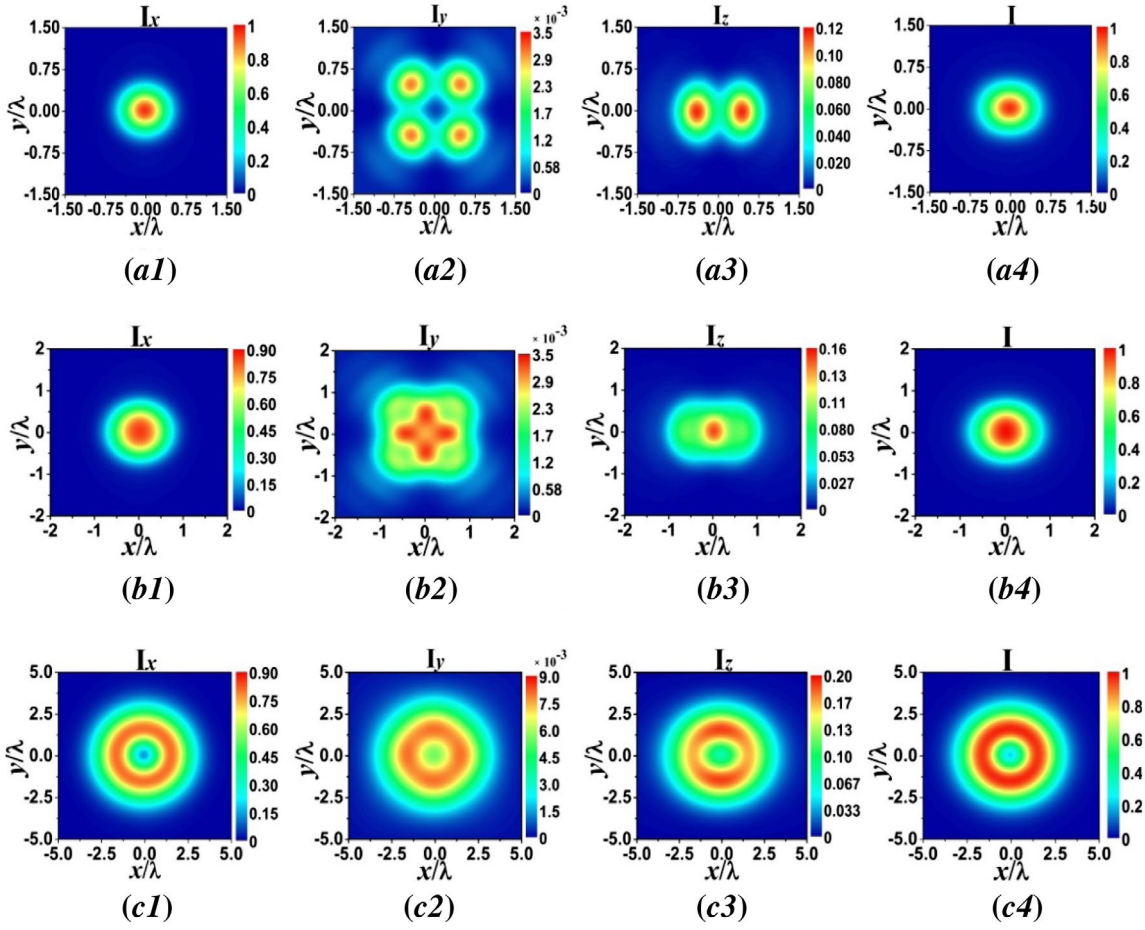

Figure 2. Normalized intensity distribution (Contour graph) of a tightly focused linearly polarized LGSM beam with the mode order $n = 1$ at the focal plane for different values of the initial spatial coherence δ_g, (*a*1)-(*a*4) $\delta_g = 10$mm, (*b*1)-(*b*4)$\delta_g = 5$mm, (*c*1)-(*c*4)$\delta_g = 1$mm, respectively. (The colour version of this figure is included in the online version of the journal.)

In the focal region, the CSD matrix of the vectorial LGSM beam is expressed as [43,45–47]

$$\vec{W}(r_1,\phi_1,r_2,\phi_2,z) = \begin{bmatrix} W_{xx}(r_1,\phi_1,r_2,\phi_2,z) & W_{xy}(r_1,\phi_1,r_2,\phi_2,z) & W_{xz}(r_1,\phi_1,r_2,\phi_2,z) \\ W_{yx}(r_1,\phi_1,r_2,\phi_2,z) & W_{yy}(r_1,\phi_1,r_2,\phi_2,z) & W_{yz}(r_1,\phi_1,r_2,\phi_2,z) \\ W_{zx}(r_1,\phi_1,r_2,\phi_2,z) & W_{zy}(r_1,\phi_1,r_2,\phi_2,z) & W_{zz}(r_1,\phi_1,r_2,\phi_2,z) \end{bmatrix} \tag{5}$$

where

$$W_{ij}(r_1,\phi_1,r_2,\phi_2,z) = \left\langle E_i^*(r_1,\phi_1,z)E_j(r_2,\phi_2,z)\right\rangle,\ i,j = x,y,z \tag{6}$$

and the elements of the CSD matrix of the LGSM beam in the focal region can be obtained with the help of the Richards–Wolf vectorial diffraction integral [46–48],

$$\begin{aligned} W_{ij}(r_1,r_2,\phi_1,\phi_2,z) = &\int_0^{\alpha}\int_0^{\alpha}\int_0^{2\pi}\int_0^{2\pi} l_0(\theta_1,\theta_2,\varphi_1,\varphi_2)\sqrt{\cos\theta_1\cos\theta_2} \\ &\times\exp\left[-ik\left(z\cos\theta_1 + r_1\sin\theta_1\cos\left(\varphi_1-\phi_1\right)\right)\right] \\ &\times\exp\left[ik\left(z\cos\theta_2 + r_2\sin\theta_2\cos\left(\varphi_2-\phi_2\right)\right)\right] \\ &\times\sin\theta_1\sin\theta_2 g_i(\theta_1,\varphi_1)g_j(\theta_2,\varphi_2)d\theta_1 d\theta_2 d\varphi_1 d\varphi_2 \end{aligned} \tag{7}$$

where

$$g_p(\theta,\varphi) = \begin{cases} \cos\theta + \sin^2\varphi(1-\cos\theta),\ p = x, \\ \cos\varphi\sin\varphi(\cos\theta - 1),\ p = y, \\ \cos\varphi\sin\theta,\ p = z, \end{cases} \tag{8}$$

where r, ϕ and z are the cylindrical coordinates of observation points, φ is the azimuthal angle of the incident beam, $k = 2\pi/\lambda$ is the wave number with λ being the wavelength of light, $\alpha = \arcsin \mathrm{NA}$ is the maximal NA angle, θ is the NA angle which varies from 0 to α. By setting $r_1 = f\sin\theta_1$, $r_2 = f\sin\theta_2$ with f being the focal length of the high-NA thin lens, the pupil apodization function of

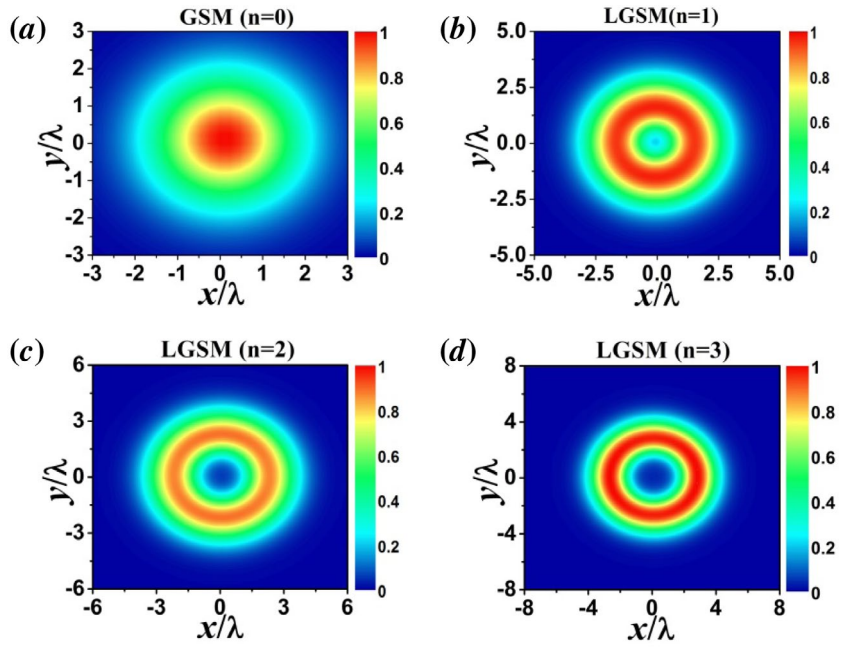

Figure 3. Normalized intensity distribution (Contour graph) of the tightly focused GSM beam and LGSM beam with the initial spatial coherence $\delta_g = 1$mmat the focal plane for different values of the mode order n, respectively. (The colour version of this figure is included in the online version of the journal.)

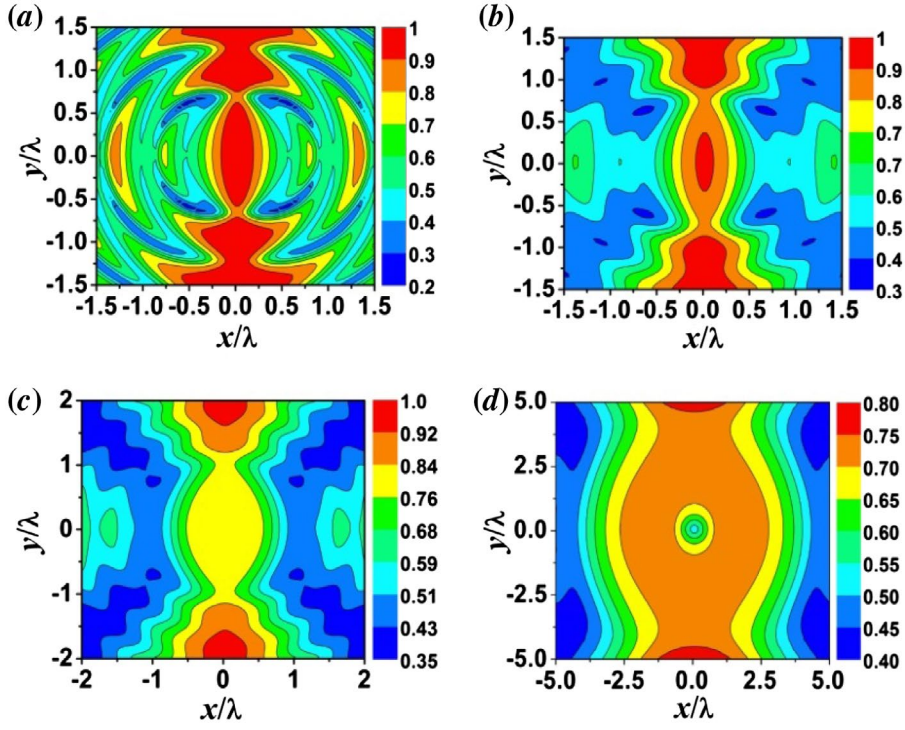

Figure 4. Degree of polarization (contour graph) of a tightly focused LGSM beam with the mode order $n = 1$ at the focal plane for different values of the initial spatial coherence δ_g, (*a*) $\delta_g = 20$mm, (*b*) $\delta_g = 10$mm, (*c*) $\delta_g = 5$mm and (*d*) $\delta_g = 1$mm, respectively. (The colour version of this figure is included in the online version of the journal.)

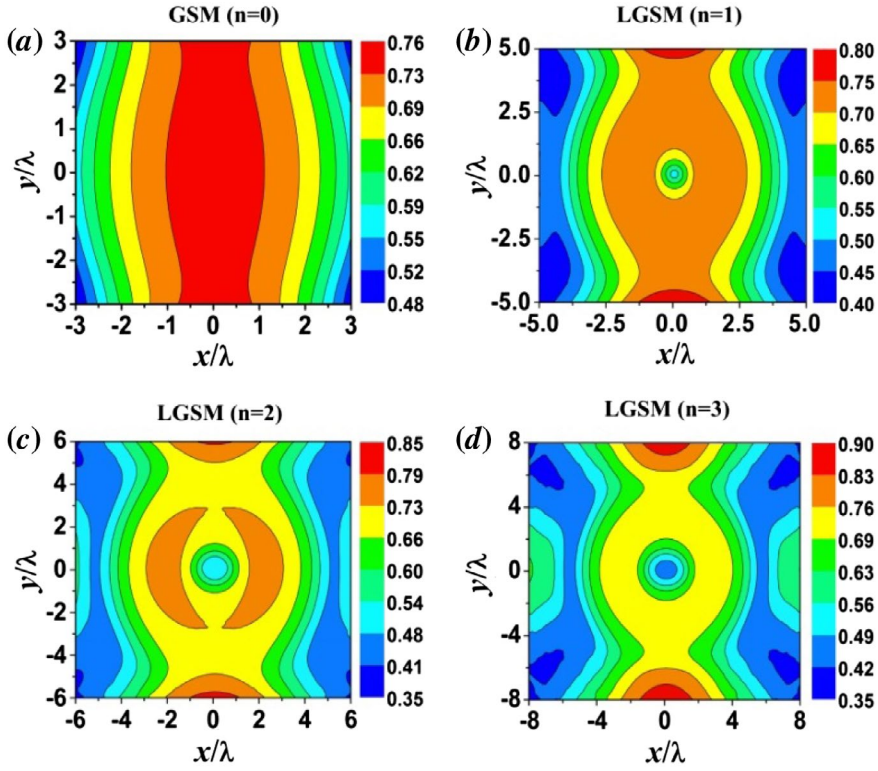

Figure 5. Degree of polarization (contour graph) of a tightly focused LGSM beam with the initial spatial coherence $\delta_g = 1\,\text{mm}$ at the focal plane for different values of the mode order n. (The colour version of this figure is included in the online version of the journal.)

a linearly polarized LGSM beam at the aperture surface in the cylindrical coordinates can be derived from Equation (4) as follows:

$$l_0(\theta_1,\theta_2,\varphi_1,\varphi_2) = \exp\left[-\frac{f^2\left(\sin^2\theta_1+\sin^2\theta_2\right)}{4\sigma_0^2}-\frac{f^2\left(\sin^2\theta_1+\sin^2\theta_2-2\sin\theta_1\sin\theta_2\cos\left(\varphi_1-\varphi_2\right)\right)}{2\delta_g^2}\right] \times L_n^0\left[\frac{f^2\left(\sin^2\theta_1+\sin^2\theta_2-2\sin\theta_1\sin\theta_2\cos\left(\varphi_1-\varphi_2\right)\right)}{2\delta_g^2}\right] \tag{9}$$

By setting $r_1 = r_2 = r$, $\phi_1 = \phi_2 = \phi$ in Equation (5), we can obtain the total intensity distribution of the tightly focused LGSM beam in the focal region as follows[6,41,43,46,47]:

$$\begin{aligned} I(r,\phi,z) &= I_x(r,\phi,z)+I_y(r,\phi,z)+I_z(r,\phi,z) \\ &= W_{xx}(r,\phi,z)+W_{yy}(r,\phi,z)+W_{zz}(r,\phi,z) \end{aligned} \tag{10}$$

The degree of polarization of the tightly focused LGSM beam in the focal region is given by [43,46,47]

$$P(r,\phi,z) = \sqrt{\frac{3}{2}\left\{\frac{I_x(r,\phi,z)^2+I_y(r,\phi,z)^2+I_z(r,\phi,z)^2}{\left[I_x(r,\phi,z)+I_y(r,\phi,z)+I_z(r,\phi,z)\right]^2}-\frac{1}{3}\right\}} \tag{11}$$

this parameter can be used to describe the depolarization of the tightly focused LGSM beam at the focal plane, when $p = 1$, the focused beam is considered as a completely polarized beam; when $p = 0$, the focused beam is a completely unpolarized beam; and when $0 < p < 1$, the focused beam is a partially polarized beam.

The degree of coherence of the tightly focused LGSM beam at an arbitrary point between any two of the three orthogonal electric field components in the focal region is defined as [43,46,47]

$$\mu_{ij}(r,\phi,z) = \frac{W_{ij}(r,\phi,z)}{\sqrt{W_{ii}(r,\phi,z)W_{jj}(r,\phi,z)}},\ \left(i,j=x,y,z\right) \tag{12}$$

The degree of coherence $\mu_{ij}(r,\phi,z)\ \left(i,j=x,y,z\right)$ is a parameter that indicates the correlation between any two of the orthogonal electric field components, and it satisfies $0 \le \left|\mu_{ij}(r,\phi,z)\right| \le 1$. $\left|\mu_{ij}(r,\phi,z)\right| = 1$ denotes complete coherence between the components, and $\left|\mu_{ij}(r,\phi,z)\right| = 0$ represents complete incoherence between the components.

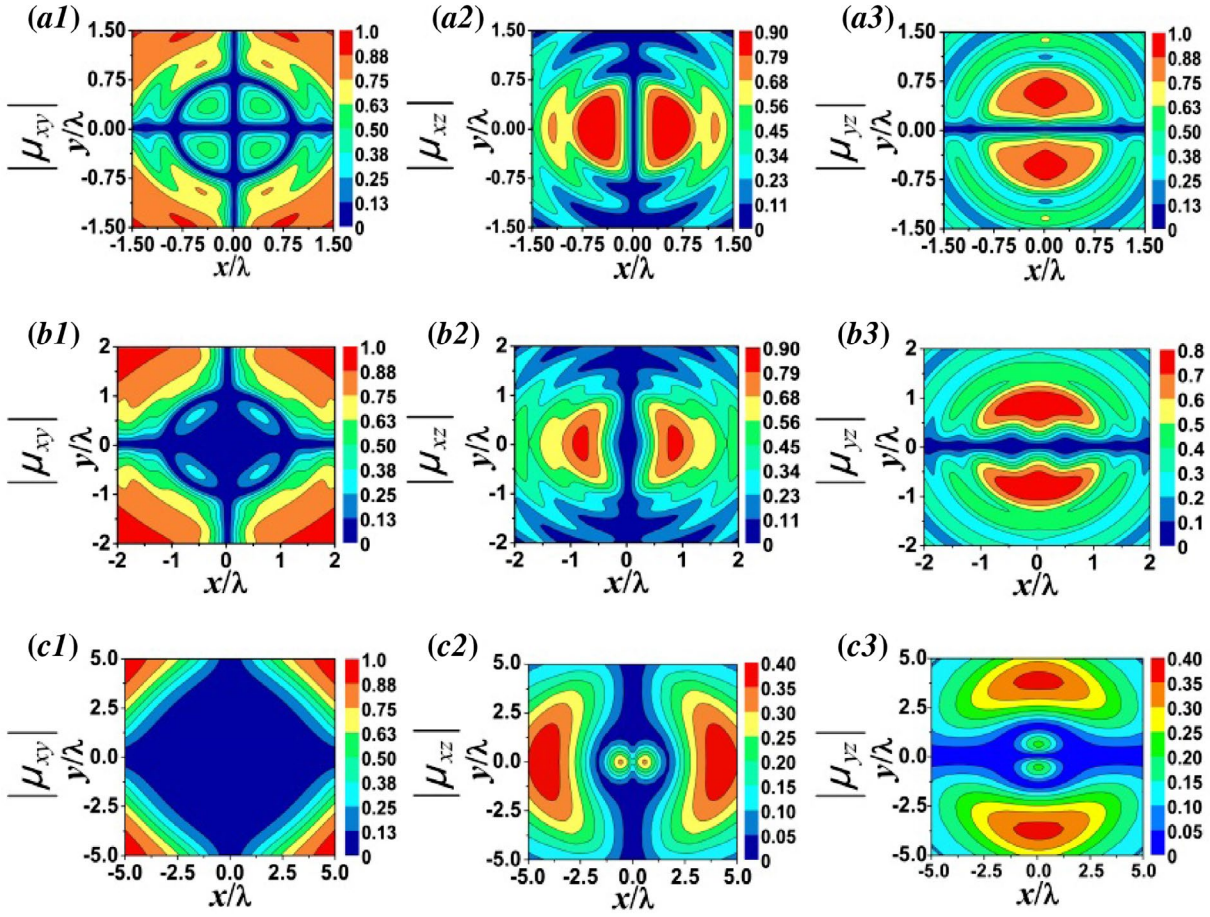

Figure 6. Contour graphs of the degree of coherences $|\mu_{xy}|$, $|\mu_{xz}|$ and $|\mu_{yz}|$ of the tightly focused LGSM beam with the mode order $n = 1$ at the focal plane for different values of the initial spatial coherence δ_g, (*a*1)-(*a*4) $\delta_g = 10$mm, (*b*1)-(*b*4)$\delta_g = 5$mm, (*c*1)-(*c*4)$\delta_g = 1$mm, respectively. (The colour version of this figure is included in the online version of the journal.)

3. Numerical results

In this section, using the formulae derived in the above section, we present some numerical results to characterize the tight focusing properties of a linearly polarized LGSM beam focused by a high-NA objective.

Figure 2 shows the intensity distribution of *x*-polarized component I_x/I_{max}, *y*-polarized component I_y/I_{max}, *z*-polarized component I_z/I_{max} and the total normalized intensity distribution I/I_{max} of a linearly polarized LGSM beam at the focal plane for three different values of the initial spatial coherence δ_g, respectively. The other parameters are chosen as $n = 1$, $\lambda = 632$nm, $\sigma_0 = 5$mm, NA = 0.9 and $f = 7$mm. From (Figures 2(*a*1–*a*4)), we can see that, for the larger initial spatial coherence (for the case of $\delta_g = 10$mm), the *x*-polarized component accounts for the main component in the total field, and the total intensity distribution I/I_{max} is of elliptical symmetry. Compared with Dong's paper [46], the intensity distributions of the LGSM beam with large initial spatial coherence δ_g are similar to that of fully coherent or partially coherent dark hollow beam with large initial spatial coherence δ_g. However, as the initial spatial coherence decreases, the total intensity distribution of the tightly focused LGSM beam in the focal plane gradually changes from an elliptical focal spot to a circular focal spot, and eventually evolves into a doughnut-shaped dark hollow beam (as the case of $\delta_g = 1$mm, see Figures (*c*1)-(*c*4)), which is quite different from that of the tightly focused partially coherent dark hollow beam or anomalous hollow beam with the conventional Schell-model correlation functions (i.e. the GSM function). The physical interpretation for this is that due to the effect of the modulated source degree of coherence with Laguerre correlation function on the intensity distributions. Therefore, we can easily control the beam profile of the tightly focused LGSM beam by varying its initial spatial coherence. This can be realized by using a rotating ground-glass disc (RGGD) in experiment, and the initial coherence length is determined by the focused beam spot size on the RGGD and the roughness of the RGGD together [22,23]. In other words, modulating the correlation function of a partially coherent beam provides a novel way for beam shaping, and thus

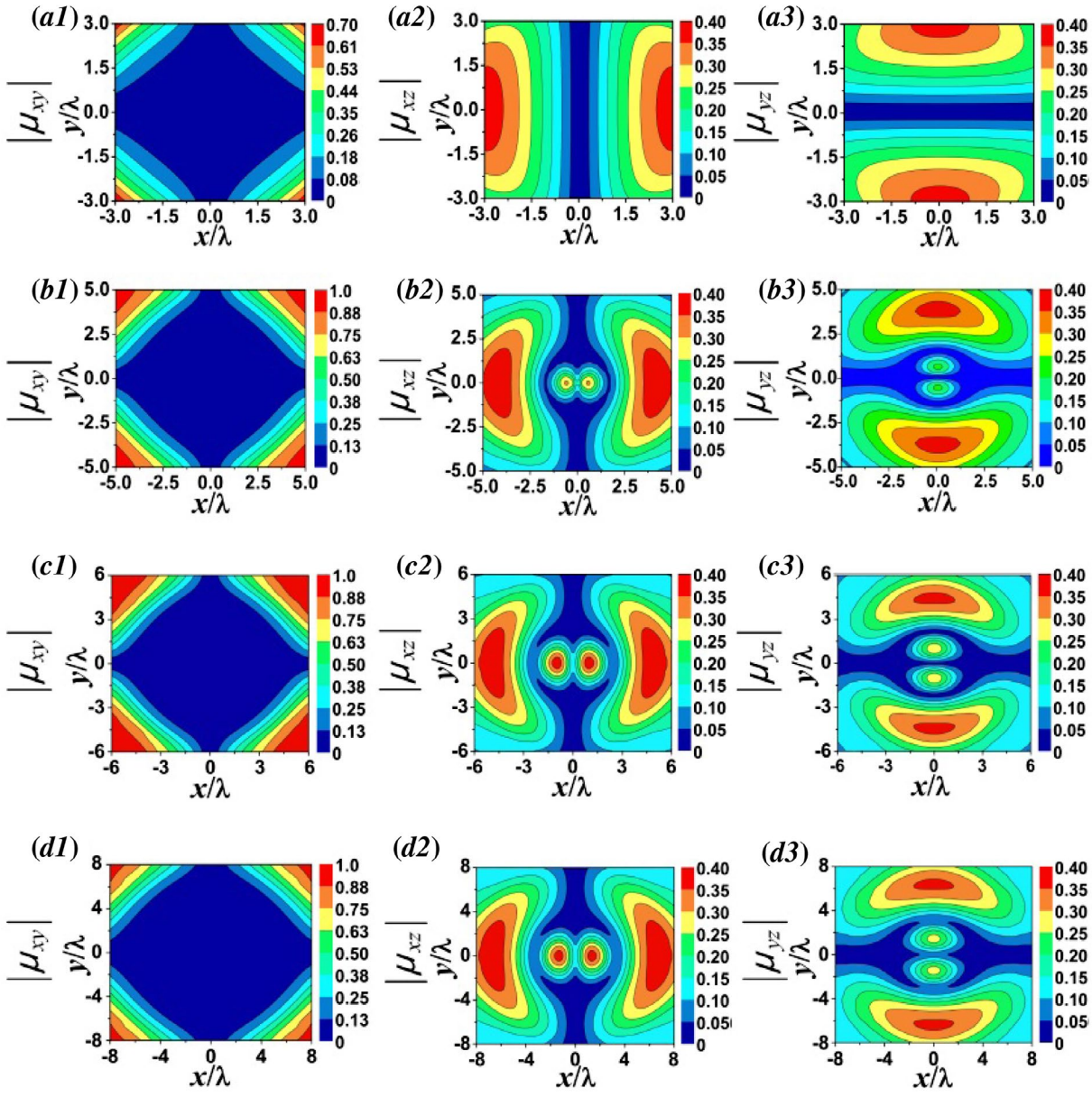

Figure 7. Contour graphs of the degree of coherences $|\mu_{xy}|$, $|\mu_{xz}|$ and $|\mu_{yz}|$ of the tightly focused LGSM beam with the initial spatial coherence $\delta_g = 1$mmat the focal plane for different values of the mode order n, ($a1$)-($a3$) GSM ($n = 0$), ($b1$)-($b3$) LGSM ($n = 1$), ($c1$)-($c3$) LGSM ($n = 2$), ($d1$)-($d3$) LGSM ($n = 3$), respectively. (The colour version of this figure is included in the online version of the journal.)

it can be expected to trap two types of particles with different refractive indices.

Figure 3 shows the effect of mode order n on the total normalized intensity distribution of the tightly focused LGSM beam with initial spatial coherence $\delta_g = 1$mmat the focal plane, and other parameters are the same as (Figure 2). Presented results are generally compared to the analogous ones obtained for the case of a conventional GSM beam (i.e. mode order $n = 0$). As shown in (Figure 3), the total intensity distribution of the GSM beam presents a circular focal spot, while the total intensity distribution of the LGSM beams exhibits a circular doughnut-shaped dark hollow profile, and its central dark size increases with the increase of mode order n.

To learn about the polarization properties of the tightly focused linearly polarized LGSM beam at the focal plane, we calculated in (Figures 4 and 5) the degree of polarization distributions (contour graph) of the LGSM beam for different values of the initial spatial coherence δ_g and mode order n, respectively. From (Figure 4), we can see that the value of the degree of polarization of the tightly focused LGSM beam does not equal 1 in most parts of the focal plane, which means that the tightly focused LGSM beam is depolarized at the focal plane. Furthermore, the depolarization is more obvious for the beam with smaller initial spatial coherence δ_g. In addition, one finds from (Figure 5) that, the distribution of the degree of polarization is also closely related with the mode order n, and the

depolarization will become more obvious for the beam with larger mode order n. Thus, we can control the polarization properties of the tightly focused LGSM beam by choosing a suitable value of the initial spatial coherence δ_g and the mode order n.

Now, we turn our attention to studying the coherence properties of the tightly focused LGSM beam at the focal plane. (Figure 6) shows the contour graphs of the degrees of coherence $|\mu_{xy}|$, $|\mu_{xz}|$ and $|\mu_{yz}|$ of the tightly focused LGSM beam with the mode order $n = 1$ at the focal plane for different values of the initial spatial coherence δ_g, the other parameters are the same as (Figure 1). As shown in (Figure 6), both the distribution of the degree of coherence and their values are closely related to the initial spatial coherence δ_g. We can control the coherence properties of a tightly focused LGSM beam by choosing suitable values of the initial spatial coherence. (Figure 7) shows the influence of the mode order n on the degree of coherence distribution of the tightly focused LGSM beam with $\delta_g = 1$mmat the focal plane. The case of the GSM beam (mode order $n = 0$) is also shown as a comparison. It is interesting to find that the distribution of the degree of coherence of the LGSM beam is quite different from that of the conventional GSM beam, while the distributions of the degree of coherence of the LGSM beam remain almost invariant as the mode order n changes.

4. Conclusion

We have studied the tight focusing properties, such as the intensity distribution, the degree of polarization and the degree of coherence, of a LGSM beam focused by a high-NA thin lens. Presented results are generally compared to the analogous ones obtained for the case of a conventional GSM beam. We have found that the tight focusing properties of the LGSM beam are quite different from that of the GSM beam, and the tight focusing properties of the LGSM beam are closely related to the initial spatial coherence δ_g and the mode order n. It is interesting to find that the LGSM beam with small initial spatial coherence can form a circular dark hollow beam at the focal plane, and its central dark size increases with the increase of mode order n. In addition, the depolarization of the tightly focused LGSM beam in the focal plane will be more obvious for the smaller initial spatial coherence δ_g and the larger mode order n. The degree of coherence of the tightly focused LGSM beam is also affected by the initial spatial coherence, but the influence of the mode order n is not evident. Our results may find applications in optical trapping for the partially coherent beams with nonconventional correlation functions.

Disclosure statement

No potential conflict of interest was reported by the authors.

Funding

This work is supported by the National Natural Science Foundation of China (NSFC) under grant numbers. 21,133,008 and 11,374,015. Acknowledgement is also made to the Thousand Youth Talents Plan, and "Interdisciplinary and Cooperative Team" of CAS.

References

[1] Mandel, L.; Wolf, E. *Opt. coherence quantum opt.*; Press: Cambridge U, 1995.
[2] Cai, Y.; He, S. *Appl. Phys. Lett.* **2006**, *89*, 041117.
[3] Ricklin, J.C.; Davidson, F.M. *J. Opt. Soc. Am. A.* **2002**, *19*, 1794–1802.
[4] Dogariu, A.; Amarande, S. *Opt. Lett.* **2003**, *28*, 10–12.
[5] Zhao, C.; Cai, Y. *Opt. Lett.* **2011**, *36*, 2251–2253.
[6] Dong, Y.; Wang, F.; Zhao, C.; Cai, Y. *Phys. Rev. A.* **2012**, *86*, 013840.
[7] Cai, Y.; Zhu, S. *Phys. Rev. E.* **2005**, *71*, 056607.
[8] Gori, F.; Santarsiero, M. *Opt. Lett.* **2007**, *32*, 3531–3533.
[9] Gori, F.; Ramírez-Sánchez, V.; Santarsiero, M.; Shirai, T.J. *J. Opt. A: Pure Appl. Opt.* **2009**, *11*, 085706.
[10] Tong, Z.; Korotkova, O. *J. Opt. Soc. Am. A* **2012**, *29*, 2154–2158.
[11] Tong, Z.; Korotkova, O. *Opt. Lett.* **2012**, *37*, 3240–3242.
[12] Gu, Y.; Gbur, G. *Opt. Lett.* **2013**, *38*, 1395–1397.
[13] Cui, S.; Chen, Z.; Zhang, L.; Pu, J. *Opt. Lett.* **2013**, *38*, 4821–4824.
[14] Mei, Z. *Opt. Lett.* **2014**, *39*, 347–350.
[15] Korotkova, O.; Sahin, S.; Shchepakina, E. *J. Opt. Soc. Am. A* **2012**, *29*, 2159–2164.
[16] Zhang, Y.; Liu, L.; Zhao, C.; Cai, Y. *Phys. Lett. A* **2014**, *378*, 750–754.
[17] Korotkova, O.; Shchepakina, E. *J. Opt.* **2014**, *16*, 045704.
[18] Yuan, Y.; Liu, X.; Wang, F.; Chen, Y.; Cai, Y.; Qu, J.; Eyyuboğlu, H.T. *Opt. Commun.* **2013**, *305*, 57–65.
[19] Mei, Z.; Korotkova, O.; Shchepakina, E. *J. Opt.* **2013**, *15*, 025705.
[20] Mei, Z.; Korotkova, O. *Opt. Lett.* **2013**, *38*, 91–93.
[21] Chen, R.; Liu, L.; Zhu, S.; Wu, G.; Wang, F.; Cai, Y. *Opt. Express.* **2014**, *22*, 1871–1883.
[22] Chen, Y.; Cai, Y. *Opt. Lett.* **2014**, *39*, 2549–2552.
[23] Chen, Y.; Wang, F.; Zhao, C.; Cai, Y. *Opt. Express* **2014**, *22*, 5826–5838.
[24] Chen, Y.; Liu, L.; Wang, F.; Zhao, C.; Cai, Y. *Opt. Express* **2014**, *22*, 13975–13987.
[25] Zhu, Z.; Liu, L.; Wang, F.; Cai, Y. *J. Opt. Soc. Am. A.* **2015**, *32*, 374–380.
[26] Cai, Y.; Chen, Y.; Wang, F. *J. Opt. Soc. Am. A.* **2014**, *31*, 2083–2096.
[27] Mei, Z.; Korotkova, O. *Opt. Lett.* **2013**, *38*, 2578–2580.
[28] Mei, Z.; Korotkova, O. *Opt. Express* **2013**, *21*, 27246–27259.
[29] Liang, C.; Wang, F.; Liu, X.; Cai, Y.; Korotkova, O. *Opt. Lett.* **2014**, *39*, 769–772.
[30] Pan, L.; Ding, C.; Wang, H. *Opt. Express* **2014**, *22*, 11670–11679.

[31] Mei, Z. *Opt. Express* **2014**, *22*, 13029–13040.
[32] Ding, C.; Liao, L.; Wang, H.; Zhang, Y.; Pan, L. *J. Opt.* **2015**, *17*, 035615.
[33] Xu, H.; Zhang, Z.; Qu, J.; Huang, W. *Opt. Express* **2014**, *22*, 22479–22489.
[34] Chen, Y.; Gu, J.; Wang, F.; Cai, Y. *Phys. Rev. A*. **2015**, *91*, 013823.
[35] Chen, Y.; Wang, F.; Liu, L.; Zhao, C.; Cai, Y.; Korotkova, O. *Phys. Rev. A* **2014**, *89*, 013801.
[36] Mei, Z. *Opt. Lett.* **2014**, *39*, 4188–4191.
[37] Mei, Z.; Mao, Y. *Opt. Express* **2014**, *22*, 22534–22546.
[38] Rydberg, C. *Opt. Lett.* **2008**, *33*, 104–106.
[39] Zhan, Q.; Leger, J. *Opt. Express* **2002**, *10*, 324–331.
[40] Kozawa, Y.; Sato, S. *Opt. Lett.* **2006**, *31*, 820–822.
[41] Hu, K.; Chen, Z.; Pu, J. *J. Opt. Soc. Am. A.* **2012**, *29*, 1099–1104.
[42] Zhan, Q. *Opt. Lett.* **2006**, *31*, 867–869.
[43] Chen, B.; Zhang, Z.; Pu, J. *J. Opt. Soc. Am. A.* **2009**, *26*, 862–869.
[44] Zhao, Y.; Edgar, J.S.; Jeffries, G.D.; McGloin, D.; Chiu, D.T. *Phys. Rev. Lett.* **2007**, *99*, 073901.
[45] Shu, J.; Chen, Z.; Pu, J. *J. Opt. Soc. Am. A.* **2013**, *30*, 916–922.
[46] Dong, Y.; Cai, Y.; Zhao, C. *Appl. Phys. B* **2011**, *105*, 405–414.
[47] Liang, C.; Zhao, C.; Zhao, C.; Wang, K.; Cai, Y. *J. Opt. Soc. Am. A.* **2014**, *31*, 2753–2758.
[48] Richards, B.; Wolf, E. *Proc. R. Soc. London, Ser. A.* **1959**, *253*, 358–379.